H_2O_2 /pH dual-responsive biomimetic nanoenzyme drugs delivery system for enhanced tumor photodynamic therapy

Xinyuan Li
The Affiliated Huai'an Hospital of Xuzhou Medical University and The Second People's Hospital of Huai'an
Qing Ji
Jiangsu University
Chao Yan
The Affiliated Huai'an Hospital of Xuzhou Medical University and The Second People's Hospital of Huai'an
Zhihui Yan
The Affiliated Huai'an Hospital of Xuzhou Medical University and The Second People's Hospital of Huai'an
Yisen Wang
Yangzhou University
Li Song (sl1035073700@163.com)
Yancheng First People's Hospital

Research Article

Keywords: phototherapy, catalase-like activity, tumor microenvironment, nano-platform

Posted Date: August 23rd, 2022

DOI: https://doi.org/10.21203/rs.3.rs-1965957/v1

Abstract

Phototherapy has been recognized as a photochemical process to treat tumor via induce cancer cells necrosis and death, with minimal invasiveness, higher selectivity and few side effects. However, the therapy effects of phototherapy are often compromised by the hypoxia, high levels of hydrogen peroxide and glutathione of tumor microenvironment (TME). Therefore, we constructed a catalase-like activity bionic metal-organic framework drugs delivery system (FA-EM@MnO_2/ZIF-8/ICG) with tumor microenvironment controllable releasing. In this system, photosensitizer Indocyanine Green (ICG) was introduced into zeolite imidazole salt skeleton 8 (ZIF-8) by one-step methods, forming ZIF-8/ICG nano-platform, which can effectively avoid ICG-induced phototoxicity and aggregation-induced quenching during transport. MnO_2 with catalase-like activity was coated on the surface of ZIF-8/ICG nano-platform, which made it have the ability of self-supplying O_2 under the condition of H_2O_2 in TME. Exposure under near-infrared light can alleviate the anoxic TME, thus improving the phototherapy efficiency. In addition, folate-functionalized erythrocyte membrane is coated on the surface of MnO_2/ZIF-8/ICG, which can endow FA-EM@MnO_2/ZIF-8/ICG with the ability of targeted drug administration and immune elimination avoidance. Therefore, FA-EM@MnO_2/ZIF-8/ICG nano-platform has the catalase-like activity, which can alleviate the oxidative stress state of TME and provide a beneficial environment for photodynamic therapy of tumor.

Introduction

Tumor is one of the major diseases that threatening human health and causing millions of deaths every year.[1] Chemotherapy and surgical resection are still the major intervention approach in clinical for tumor therapy nowadays.[2–3] However, surgical resection and chemotherapy suffered from the high risk of tumor recurrence and cased seriously damage to normal organs and tissues. In order to enhance tumor therapy effects and avoid unnecessary side effects to normal tissues, various novel tumor therapy approach have been developed, such as starvation therapy (ST), photothermal therapy (PTT), photodynamic therapy (PDT), and sonodynamic therapy (SNT).[4–6]

Due to tumor tissues lacking autonomous regulatory ability leading tumor tissues to be a relative heat reservoir, thus PTT and PDT have the inherent advantages in the field of tumor therapy.[7–8] However, cancer cells grown fast as well as distorted blood vessels would lead tumor tissues lack adequate oxygen supply, in the state of oxidative stress as well as acidification condition leading tumor therapy effects are compromised.[9] In addition, using PTT alone may cause seriously damage to surround tissues and organs, due to cancer cells need high temperature to kill.[10]

With the development of biomedical, various kings of photo-thermal material and photosensitizers (PSs) have been widely applied in the tumor therapy. Among them, indocyanine green (ICG), as the ideal medical diagnostic agent, is approved by Food and Drug Administration (FDA) due to its low toxicity.[11] In addition, ICG has strong fluorescence characteristics and near-infrared absorption ability, which can

penetrate into deep tissues, so that ICG can be applied to photothermal therapy triggered by near-infrared light (NIR) guided by fluorescence imaging.[12–13] Nevertheless, ICG is inevitable distributed around the entire body, especially in skin, and also cause phototoxicity to them after injection.[2] What's more, ICG still has aggregation-induced quenching phenomenon in the process of blood circulation, which will lead to low photothermal conversion efficiency, thus reducing the therapeutic efficiency.[14] Various strategies have been developed to overcome these drawbacks associated with ICG, but the result is disappointing.

According to literature reports, metal-organic frameworks (MOFs) have a large surface area, finely tunable pore shape and size, excellent biodegradability, and the surface is easily modified, which has been widely applied in the field of biomedical, especially as drugs delivery system for disease therapy.[15–16] As drug delivery system, MOFs has many incomparable advantages, but its application is widely restricted by some prominent problems, such as difficult to achieve on-demand release, easy to be cleared by body's immune system and unsatisfactory targeted delivery capability.[17–19] Zeolite Imidazole Skeleton 8 (ZIF-8), as the typical MOFs, is easily decomposed in acid tumor microenvironment (TME), due to their metal-ligand interaction is very unstable.[20] Especially, the synthesis progress of ZIF-8 is very mild, which can effectively maintain the biological activity of drugs, the surface of ZIF-8 is easy to be modified to improve its biocompatibility and tumor treatment effects at the same time.[21]

In summary, we constructed H_2O_2/pH-responsive drugs nano-platform based on ZIF-8 (FA-EM@MnO_2/ZIF-8/ICG) with catalase-like activity for photothermal therapy of tumors. As shown in Scheme 1, FA-EM@MnO_2/ZIF-8/ICG was prepared by biomimetic mineralization and coprecipitation reaction between Zn^{2+} ion and 2-methylimidazole to load ICG (ZIF-8/ICG), whose surface was coated with a layer of MnO_2 (MnO_2/ZIF-8/ICG), and then MnO_2/ZIF-8/ICG exterior surface was further cloaked with folic acid modified erythrocyte membrane. Thanks to the fact that manganese dioxide has nano-enzyme-like activity, the obtained FA-EM@MnO_2/ZIF-8/ICG can alleviate the oxidative stress of tumor tissues by catalyzing and decomposing endogenous H_2O_2 into O_2, and correspondingly reduce the hypoxia condition of tumor to improve the results of photodynamic therapy.[22] Meanwhile, folic acid-functionalized erythrocyte membrane (FA-EM) was further coated into the surface of MnO_2/ZIF-8/ICG, which can endow FA-EM@MnO_2/ZIF-8/ICG targeted delivery to the tumor tissues via folic acid receptors, and avoid eliminated by body immune system to prolong their blood circulation.[23] Therefore, our designed FA-EM@MnO_2/ZIF-8/ICG nano-platform with dual pH and H_2O_2 responses can realize the controlled release of ICG in time and space. By simultaneously targeting delivery, avoiding eliminate by body immune system, continuously supplying O_2, ameliorating oxidative stress, and overcoming hypoxia TME. Thus, our FA-EM@MnO_2/ZIF-8/ICG nano-platform provided an instructive TME for improving tumor PDT.

Experimental Section

Materials and Reagents

$KMnO_4$, hydrogen peroxide, 2-methylimidazole and $Zn(NO_3)_2{\cdot}6H_2O$ purchased from Sinopharm Chemical Reagent (Beijing, China). Indocyanine green (ICG), 4',6-diamidino-2-phenylindole (DAPI), glutathione (GSH, reduced), cell counting kit-8 (CCK-8), 1,3-diphenylisobenzofuran (DPBF), $[Ru(dpp)_3]Cl_2$ (RDPP), 2',7'-dichlorofluorescein diacetate (DCFH-DA) and 1,2-distearoyl-sn-glycero-3-phosphoethanolamine-N-[folate (polyethylene glycol)-2000] (DSPE-PEG-FA) bought from Aladdin (Shanghai, China). Fetal bovine serum (FBS), dulbecco's modified eagle medium (DMEM), phosphate buffer (PBS) and 1640 medium purchased from Gibco (Shanghai, China). All chemicals were used in this work without further purification.

Apparatus and Procedures

Transmission electron microscopy (TEM) images were obtained on a transmission electron microscope (JEOL 2100, Japan). X-ray powder diffraction (XRD) measurement, Brunauer-Emmett-Teller (BET) surface area, ζ-potential measurements and mapping were performed from on an X-ray diffractometer (GBC MMA Instrument), N_2 adsorption-desorption isotherms (NovaWin 1000e, USA), and a NanoBrook Omni (Brookhaven, USA), respectively. Infrared thermal photos and temperature changes were recorded on the infrared thermal camera (HT-19, Guangzhou, China). 808 nm near-infrared irradiation was performed by a fiber-coupled NIR laser (MDL-N-808 nm-10W, Beijing Laserwave OptoElectronics Technology Co., Ltd., Beijing, China). Confocal laser scanning microscopy (CLSM, Nikon, Japan) was performed to detect cytophagocytic behavior.

Synthesis of ZIF-8/ICG

ZIF-8/ICG nano-platform was prepared according to previous methods.[24] Briefly, $Zn(NO_3)_2{\cdot}6H_2O$ (1470 mg) and ICG (100 mg) were added into the 10 mL PBS solution and stirring for 15 min to obtain homogeneous solution A. Then, 2-methylimidazole (810 mg) was also added into the 10 mL PBS stirring at 800 rpm for 15 min to obtain solution B. Finally, solution B was slowly dropped into the solution A, and then the mixed solution was continued stirring at 800 rpm for 15 min. The obtained ZIF-8/ICG was washed with PBS for three times, and the supernatant solution was kept for confirming the ICG content through high-performance liquid chromatography (HPLC).

Synthesis of MnO_2/ZIF-8/ICG

10 mg ZIF-8/ICG was dispersed in 10 mL PBS solution and ultra-sonicated for 10 min to obtain homogeneous dispersion. Then, 10 mL aqueous solution of $KMnO_4$ solution (1 mg/mL) was added dropwise and stirred at 800 rpm for 4 h. Then, the color of ZIF-8/ICG turned into brown after MnO_2 successful coated into the surface of ZIF-8/ICG.[25]

Synthesis of FA-EM@MnO_2/ZIF-8/ICG

Erythrocyte membrane (EM) vesicles were obtained according to the previous methods with some modification.[26] Firstly, erythrocytes was collected from BALB/c mice fresh blood and washed with PBS for sever times to remove plasma and unwanted cells until the supernatant became colorless. Secondly,

the obtained erythrocytes were immersed into 5mL ultrapure water at 4℃ for 2 h, during that the intracellular components inside of the erythrocytes were released. Thirdly, the products were washed with PBS for three times and followed by extrusion through polycarbonate membranes. Lastly, EM was further dispersed in PBS solution and stored at -80 ℃ before used.

To obtained the final products FA-EM@MnO_2/ZIF-8/ICG. Briefly, DSPE-PEG-FA (10 mg) was added into the EM solution and continuous stirred at 4℃ for 12h.[27] Then, the products FA modified EM (FA-EM) was collected by centrifuging (15000 rpm, 5 min) and washed with PBS for three times. Finally, the obtained FA-EM was mixed with MnO_2/ZIF-8/ICG followed by stirred at 1000 rpm for 24 h; and then the products were washed with PBS for three times and centrifuged at 4000 rpm to removed free FA-EM.[28]

Cellular uptake

First, RAW264.7 cells (mouse macrophage cells), 4T1 cells (mouse breast cancer cells) and GES-1 cells (human gastric mucosa cells) were respectively seeded into six-well plate and incubated for 24 h. Different formulation of nano-platform (100 μg/mL) were added into each well and incubated for another 3 h. Then, the cells were fixed with 4% paraformaldehyde and added DAPI for 15 min to label the nucleus. Finally, cells were washed with PBS for three times and observed by a confocal microscope.[29-30]

Evaluation of O_2 generation

The concentration of extracellular oxygen, which was generated in the FA-EM@MnO_2/ZIF-8/ICG was quantified by a dissolved oxygen meter.[31] Briefly, FA-EM@MnO_2/ZIF-8/ICG dispersion was putted into 50 mL beaker, and H_2O_2 (100 μL, 30 mM) was added. Then, the dissolved oxygen meter probe was inserted into the mixing solution to detect oxygen concentration with continue stirring. Then, PBS, H_2O_2 solution, and MnO_2/ZIF-8/ICG + H_2O_2 were applied as control. Additionally, O_2 generation within the cells were monitored through RDPP, whose red fluorescence signal can be quenched by O_2. Briefly, 4T1 cells were incubated with 10 μM RDPP for 4 h at 37°C. Then, 4T1 cells were treated with PBS, H_2O_2, FA-EM@MnO_2/ZIF-8/ICG and FA-EM@MnO_2/ZIF-8/ICG + H_2O_2, and incubated for another 4 h. Finally, 4T1 cells were washed with PBS for three times and observed through fluorescence microscopy.[32]

Releasing behavior of ICG

To investigate the ICG releasing behavior from FA-EM@MnO_2/ZIF-8/ICG nano-platform, 10 mg FA-EM@MnO_2/ZIF-8/ICG nano-platform was immersed into normal physiological environment (pH = 7.4) and simulate tumor microenvironment (TEM, pH = 5.5, 10 mM GSH, 30 μM H_2O_2,), respectively. The different FA-EM@MnO_2/ZIF-8/ICG dispersion solution were incubated at 37℃ on a horizontal shaker with 300 rpm. At designed points, 3 mL supernatant solution was withdrawn and the ICG released content was determined by fluorescence spectroscopic instrument.[14, 33]

Photothermal performance measurements

The FA-EM@MnO_2/ZIF-8/ICG dispersion solution (ICG concentration: 150 and 200 μg/mL), and MnO_2/ZIF-8/ICG (ICG concentration: 200 μg/mL) were exposed under 808 nm NIR irradiation with 1.5 W/cm^2 or 2.0 W/cm^2 for 600 s and recorded by infrared thermal image, respectively. PBS solution was set as control group.[5, 34]

Cytotoxicity assay

4T1 cells and GES-1 cells were respectively seeded into 96-well plates with the density of 1 × 10^4 cells for each well and incubated for 12h, then treated with different concentrations (0, 50, 100, 150 and 200 μg/mL, as an equivalent dosage of ICG) of different kinds of nano-platform (ZIF-8/ICG, MnO_2/ZIF-8/ICG, and FA-EM@ MnO_2/ZIF-8/ICG) with NIR irradiation, or with PBS and PBS + NIR as control. After 48 h incubation, cell counting kit-8 (CCK-8) were utilized to analysis the cells viability.[35-36]

Detection of reactive oxygen species

DPBF as the chemical probe was utilized to detect the reactive oxygen species (ROS) generation of FA-EM@MnO_2/ZIF-8/ICG nano-platform with different treatment, which could react with DPBF to lead an irreversibly reduction in the DPBF absorbance.[37-38] Typically, FA-EM@MnO_2/ZIF-8/ICG and DPBF were respectively added into 2 mL DPBF/DMSO (1:1) and exposed under 808nm NIR irradiation (2.0 W/cm^2). At the designed time point, the absorbance of DPBF near 417 nm was recorded by UV-visible spectrophotometer. The absorbance value of DPBF in H_2O_2 solution, FA-EM@MnO_2/ZIF-8/ICG + NIR, and FA-EM@MnO_2/ZIF-8/ICG + H_2O_2 were also recorded as the control.

Besides, ROS generation within the cells were monitored through a cell-permeable dye-DCFH-DA. As well all know, DCFH-DA was nonfluorescent signal at normal condition, which can be oxidized into stronger green fluorescent 2,7-dichlorofluorescin (DCF) by ROS.[39] First, 4T1 cells were seeded into 12-well plate and treated with different approach (blank, NIR irradiation, H_2O_2, FA-EM@MnO_2/ZIF-8/ICG + NIR, FA-EM@MnO_2/ZIF-8/ICG + H_2O_2, and FA-EM@MnO_2/ZIF-8/ICG + H_2O_2 + NIR. After 6 h incubated, the old medium was discarded and supplanted with fresh medium and exposed under 808 nm NIR irradiation with the power of 2.0 W/cm^2 for 10 min. Then, the chemical probe of DCFH-DA was added and incubated for 30 min. Lastly, 4T1 cells were washed with PBS for three times and detected by fluorescence microscopy.

In vivo therapeutic effects

5×10^6 4T1 cells were injected into the right back of BALB/c female mice to establish the subcutaneous 4T1 tumor model.[40] All animal experiments were approved according to the Institutional Animal Care and Use Committee of Yangzhou University. When the tumor volume reached for about 50 mm^3, the mice were intravenously treated with PBS or different kinds nano-platform once every 3d for a total of five times accompanied with NIR irradiation. The mice were randomly divided into five groups (n=6) as the

following methods: 1) PBS, 2) PBS+NIR, 3) ZIF-8/ICG+NIR, 4) MnO_2/ ZIF-8/ICG+NIR, 5) FA-EM@MnO_2/ZIF-8/ICG+NIR. For mice that received photothermal therapy, at 24 h after each injection the mice were exposed under 808 nm NIR irradiation at 2.0 W/cm^2 for 10 min. Tumor volume and body weight of each mouse was monitored every three days during the whole assays. After 15 d treatment, the mice were euthanized for further investigation. The tumor volume was evaluated as following formula: Tumor volume (mm^3) = 1/2 × $width^2$ × length.[41]

Histological analysis

To explore the therapeutic effects and the biocompatibility of FA-EM@MnO_2/ZIF-8/ICG, the tumors and major organs (heart, liver, spleen, lung and kidney) of the mice were dissected and sectioned for transferase-mediated deoxyuridine triphosphate nick end labeling (TUNEL) staining and H&E staining.[42] All the histological was carried out by Servicebio (Wuhan, China).

Statistical analysis

All the experiment data were analyzed by OriginPro and SPSS.17.0. All the error bars indicated mean ± standard deviation (mean ± SD). The student's *t*-test was applied for statistical analysis. The *p* value of < 0.05 was considered statistically significant. *$p < 0.05$, **$p < 0.01$, ***$p < 0.001$.

Results And Discussion

By biomimetic mineralization and coprecipitation, 2-ICA and Zn^{2+} were directly mixed and ZIF-8/ICG nano-platform were synthesized in one step. We found that the size of ZIF-8 nano-platform is about 60 nm, and the surface area is about 996.37 m^2/g, which indicated that ZIF-8 nano-platform is ideal for drugs loading in tumor therapy (Fig 1a and b). XPS results show that ZIF-8 nano-platform was mainly composed with zinc, nitrogen and carbon, their percentages are about 68.86%, 27.12% and 10.02% respectively (Fig 1c). After the surface of ZIF-8 as modified with MnO_2, the size and the morphology of MnO_2/ZIF-8 were not significantly changed (Fig 1d and e). However, XPS results show that MnO_2/ZIF-8 is mainly composed of zinc, nitrogen, carbon, oxygen and manganese, they are uniformly dispersed in the nano-platform, with mass percentages of 57.85%, 24.94%, 9.22%, 7.38% and 0.63% respectively (Fig 1e and i). In order to improve the biocompatibility and targeting of MnO_2/ZIF-8, FA-EM was modified on the surface of MnO_2/ZIF-8. TEM showed that the size of FA-EM@ MnO_2/ZIF-8 became larger, but the morphology had no obvious change (Fig 1f). Gel electrophoresis results showed that the protein composition of FA-EM@MnO_2/ZIF-8 nano-platform kept well with that of pure EM, which indicated that the membrane protein of FA-EM fused to the surface of MnO_2/ZIF-8 nano-platform was well preserved (Fig 1g) From Fig 1h, power X-ray diffraction (XRD) diagram shows that all the characteristic peaks of two samples (MnO_2/ZIF-8, and FA-EM@MnO_2/ZIF-8) are very similar to those of pure ZIF-8. The above results show that we successfully synthesized FA-EM@MnO_2/ZIF-8 nano-platform.

The ZIF-8/ICG nano-platform was prepared via directly self-assembly of 2-ICA and Zn^{2+} in the present of ICG. Thus, zeta potential measurement was utilized to analysis the products formed at any synthesis stages (Fig 2a). Compared with the data of pure ZIF-8, the zeta potential of ZIF-8/ICG nano-platform increased slightly, which indicated that ICG molecule were successfully incorporated into ZIF-8 crystals. The zeta potential of MnO_2/ZIF-8/ICG nano-platform also increased when MnO_2 was successfully modified on the surface of ZIF-8, but when FA-EM was modified on the surface of MnO_2/ZIF-8/ICG nano-platform, the positive zeta potential of MnO_2/ZIF-8/ICG became negative. In addition, the hydrodynamic diameter measurements were made to study the products formed at different synthesis stages (Fig 2b). The size of FA-EM@MnO_2/ZIF-8/ICG nano-platform is consistent with the measurement results of transmission electron microscope.

High drugs loading capacity and tumor tissues on-demand releasing are the key factor to enhance therapeutic effect and avoid unnecessary side effects. ZIF-8 was expected to be an excellent nano-platform for drugs loading and delivery because of its huge surface area. Fig 2c shows that the loading efficiency of ZIF-8 for ICG, a typical photosensitizer for tumor photothermal therapy with green fluorescence, reached for about 60% (ZIF-8/ICG), as determined by the fluorescence signal of ICG. The zeta potential also confirmed the successful loading of ICG. *In vitro* releasing behavior of ICG from FA-EM@MnO_2/ZIF-8/ICG was evaluated in simulated (pH = 7.4) and TME-simulating environment (pH = 5.5, 10 mM GSH, 30 μM H_2O_2). As shown in Fig. 2d, under physiological conditions (pH = 7.4), only about 10% ICG was released after 50 hours. However, in TME-simulating environment, more than 40% of ICG was released after 24 hours, and about 75% of ICG was released after 50 hours. This was due to the accumulation of H_2O_2 on the surface of EM, which promoted the formation of pores on the surface of EM and promoted the solution to enter the center of FA-EM@MnO_2/ZIF-8/ICG.[43] Due to the ZIF-8 is prone to decompose under acidic environment, which can make ZIF-8 structure collapsed leading ICG releasing in the TME.[44] Thus, FA-EM@MnO_2/ZIF-8/ICG could be acted as an ideal tumor therapy platform.

It is worth noting that ICG is the typical PS, and it has excellent photothermal conversion efficiency when exposed to NIR.[45] Therefore, the photothermal conversion effects of FA-EM@MnO_2/ZIF-8/ICG was also evaluated via irradiation with NIR, showing super penetration into normal tissues, and the damage was negligible. Then, FA-EM@MnO_2/ZIF-8/ICG dispersion solution with different concentrations (ICG concentration: 150 and 200 μg/mL) were irradiated at NIR with the power of 1.5 or 2.0 W/cm^2. The photothermal conversion shows obvious dependence on time, concentration and radiation power. When the temperature increased for about 32.8 ℃ at the concentration of 200 μg/mL with the power of 2.0 W/cm^2 for 10 min, the photothermal conversion efficiency (η) for about 40.1%, which was suitable for tumor therapy than traditional phototheramal agents (Fig 2g).[46] It should be noted that MnO_2/ZIF-8/ICG and FA-EM@MnO_2/ZIF-8/ICG nano-platform displayed similar temperature changes under the same conditions, which indicated that FA-EM camouflaged had no obviously influence of the irradiation absorption of MnO_2/ZIF-8/ICG (Fig 2e). In addition, FA-EM@MnO_2/ZIF-8/ICG dispersion shown outstanding photothermal stability after treated with five turn on/off cycles, indicative of excellent

reversible temperature changes (Fig 2f). Therefore, the obtained FA-EM@MnO_2/ZIF-8/ICG nano-platform shown enormous potential as a photothermal agent for antitumor therapy.

In the presence of NIR radiation, the cytotoxicity of ZIF-8/ICG nano-platform with different preparations of different kinds of cells was tested *in vitro*. For GES-1 cells, no significant toxicity of ZIF-8, manganese dioxide /ZIF-8/ICG and FAFA- manganese dioxide /ZIF-8/ICG was detected until the equivalent ICG dose reached 200 μg/mL (Fig 2h), after 10 minutes of near-infrared radiation, which was also the same dose selected for the in vitro analysis of 4T1 cells. 4T1 cells were incubated for 3 hours with each nano-platform before being irradiated for 10 minutes. Comparing with GES-1 cells viability, the 4T1 cells killing efficiency of each nano-platform exhibited ICG dose-dependent cytotoxicity in the presence of NIR irradiation, and only about 38.2% 4T1 cells viability under NIR irradiation with the power of 2.0 W/cm^2 at the dose of FA- FA-EM@MnO_2/ZIF-8/ICG for 200 μg/mL. Therefore, FA-EM@MnO_2/ZIF-8/ICG can effectively kill cancer cells as a nano-platform, and avoid unnecessary side effects to normal cells.

To gain insight into the details of FA-EM@MnO_2/ZIF-8/ICG nano-platform has high cytotoxicity to cancer cells than normal cells upon being exposed under NIR irradiation. CLSM analysis showed that the FA-EM@MnO_2/ZIF-8/ICG nano-platform was swallowed up by 4T1 cells more than GES-1 cells. The fluorescence intensity of ICG in 4T1 cells was approximately four-fold stronger than that of normal GES-1 cells (Fig 3a). This is because FA-EM@MnO_2/ZIF-8/ICG nano-platform can specially bind with folate receptor (FA) which is over expressed on the surface of 4T1 cells, resulting in more FA-EM@MnO_2/ZIF-8/ICG nano-platform phagocytosis by 4T1 cells. It has been reported in many literatures that nanoparticles coating erythrocyte membrane (EM) can give bionic nanoparticles longer blood circulation and avoid being cleared by the immune system.[47-48] Therefore, we further studied the effect of EM timing on macrophage phagocytosis. From CLSM results shown that macrophage cells exhibited significantly decreased binding or internalization of EM@MnO_2/ZIF-8/ICG nano-platform compared to that of MnO_2/ZIF-8/ICG nano-platform. This was consistent with the previous studies, which means EM clock control can reduce the clearance of nano-materials by the reticuloendothelial systems, and it is proved that EM camouflage can increase the circulation time of ZIF-8 nano-platform *in vivo*.[49] It should be pointed out that the fluorescence intensity of FA-EM@MnO_2/ZIF-8/ICG nano-platform becomes slightly stronger than that of EM@MnO_2/ZIF-8/ICG nano-platform, which indicates that the stealth effects of EM is minimally damaged after FA modification of EM surface. The above results indicate that FA-EM@MnO_2/ZIF-8/ICG nano-platform has the ability of targeted delivery and invisibility in blood circulation, which can enhance tumor treatment effects.

Weak acidity, hypoxia, increased H_2O_2 levels, and high concentration of GSH are the typical characteristics of the TME.[50-51] It is reported that MnO_2 has catalase-like activity can trigger O_2 generation from H_2O_2.[52] In order to study the O_2 generation capacity of FA-EM@MnO_2/ZIF-8/ICG nano-platform in H_2O_2 environment, more O_2 could be detected upon MnO_2/ZIF-8/ICG and FA-EM@MnO_2/ZIF-8/ICG nano-platform immersed into the H_2O_2 solution compared with MnO_2/ZIF-8/ICG and FA-

EM@MnO_2/ZIF-8/ICG nano-platform immersed into PBS solution by a dissolved oxygen meter (Fig 4a). Additionally, more bullule can be detected once MnO_2/ZIF-8/ICG and FA-EM@MnO_2/ZIF-8/ICG nano-platform immersed into H_2O_2 solution (Fig 4b). It should be noted that FA-EM@MnO_2/ZIF-8/ICG nano-platform can't produce O_2 rapidly at the begin time than MnO_2/ZIF-8/ICG, which would ascribe to the H_2O_2 solution infiltrated through the FA-EM and entered into the core area of FA-EM@MnO_2/ZIF-8/ICG to react with MnO_2, but FA-EM cloaked can't effect FA-EM@MnO_2/ZIF-8/ICG catalase-like activity. In addition, RDPP as the typical oxygen-sensitive probe, whose fluorescence can be quenched in O_2 environment.[53] As expected, the fluorescence intensity of RDPP was significantly decreased upon FA-EM@MnO_2/ZIF-8/ICG nano-platform immersed into the H_2O_2 solution with time gone, which indicative that O_2 was gradually generated in the presence of both H_2O_2 and FA-EM@MnO_2/ZIF-8/ICG nano-platform (Fig 4f). As the control, O_2 can hardly detected in the solution only containing PBS, H_2O_2, and FA-EM@MnO_2/ZIF-8/ICG dispersion solution (Fig 4c-e). Besides, intracellular fluorescence signal of RDPP was further tested through 4T1 cells incubated with FA-EM@MnO_2/ZIF-8/ICG. From Fig 4g shown, the fluorescence intensity of RDPP was quenched upon 4T1 cells incubated with FA-EM@MnO_2/ZIF-8/ICG nano-platform, and the fluorescence intensity was almost quenched once H_2O_2 added. In contrast, 4T1cells without FA-EM@MnO_2/ZIF-8/ICG nano-platform did not show any obviously fluorescence quenched (Fig 4g). The above results clearly indicated that MnO_2 in FA-EM@MnO_2/ZIF-8/ICG can catalyze the H_2O_2-triggered intracellular O_2 production, so as to overcome the hypoxia TME and provide more O_2 for subsequent photodynamic therapy.

In order to investigate whether reactive oxygen (ROS), such as hydroxyl radical ($\cdot OH$), and singlet oxygen ($^1O_2$) could be produced in the presence of FA-EM@MnO_2/ZIF-8/ICG at TME with or without NIR irradiation. As a probe of extracellular ROS, DPBF can be oxidized by ROS, and its UV-vis absorption decreases.[54] According to Fig 5a-d, the UV-Vis absorption values of DPBF in different environments have decreased. Obviously, the UV-visible absorption value of DPBF in FA-EM@MnO_2/ZIF-8/ICG + H_2O_2 + NIR irradiation group decreased significantly, which indicates that the ROS was the highest. In addition, DCFH-DA was used as an indicator to detect the production of intracellular ROS through different treatments. DCFH-DA can be oxidized by intracellular ROS into stronger green fluorescent DCF.[55] By contrast with PBS group (1), treated with NIR irradiation only group (2), and H_2O_2 group (3), a green fluorescence signal was clearly presented after 4T1 cells treated with FA-EM@MnO_2/ZIF-8/ICG or FA-EM@MnO_2/ZIF-8/ICG + NIR. Moreover, the green fluorescence signal became stronger with H_2O_2 added, which was ascribed to FA-EM@MnO_2/ZIF-8/ICG was beneficial to trigger the catalytic activity to produce more O_2 and OH, and then improve the PDT process under NIR irradiation (Fig 4e). These results correspond with the DPBF results, confirming that the obtained FA-EM@MnO_2/ZIF-8/ICG nano-platform has the catalase-like activity can produce more O_2 and ROS to overcome hypoxia TME with the existence of H_2O_2 and improve PDT efficacy.

The excellent stimulation response behavior and anti-tumor effects of FA-EM@MnO_2/ZIF-8/ICG forced us to further evaluate its anti-tumor activity *in vitro*. In order to explore the appropriate time for tumor treatment, the *in vivo* distribution of FA-EM@MnO_2/ZIF-8/ICG nano-platform at the designed time was analyzed by luminescence imaging and magnetic resonance imaging (MRI). Comparing with MnO_2/ZIF-8/ICG nano-platform, after FA-EM@MnO_2/ZIF-8/ICG was injected into the 4T1 xenograft tumor mouse model, more ICG fluorescence signals were observed in the tumor area, and the fluorescence signal gradually weakened after 24 hours of injection (Fig 6a). The MRI results also confirmed that more FA-EM@MnO_2/ZIF-8/ICG nano-platforms accumulated at the tumor areas 24 h after the injection, which indicated that FA-EM@MnO_2/ZIF-8/ICG nano-platforms could achieve the tumor-targeted delivery of ICG through the folate receptors overexpressed on the tumor cell surface (Fig 6b).Therefore, above results indicate that FA-EM@MnO_2/ZIF-8/ICG nano-platform could be effectively delivered to the tumor areas 24 h after injection, and the nonspecific uptake by other organs can be avoided during the transport process.

Therefore, we established a 4T1 xenograft tumor model to detect the anti-tumor effects of FA-EM@MnO_2/ZIF-8/ICG nano-platform under NIR irradiation. NIR irradiation was performed with the power of 2.0 W/cm^2 every three days after 24 h post-injection. As shown in Fig 7a-c, the tumor volume of different nano-platforms (ZIF-8/ICG, MnO_2/ZIF-8/ICG, and FA-EM@MnO_2/ZIF-8/ICG) after treatment showed some degree of inhibition. Especially, when FA-EM@MnO_2/ZIF-8/ICG nano-platform treated mice were exposed to near infrared radiation, the tumor volume decreased significantly, which was attributed to the tumor-targeted delivery behavior of FA and the immune escape ability of EM on the surface of FA-EM@MnO_2/ZIF-8/ICG nano-platform. Once in TEM, high levels of H_2O_2 can trigger the production of O_2 to improve ameliorate hypoxia TME and provide more ROS to kill cancer cells under NIR irradiation. What's more, compared with PBS and PBS+NIR irradiation group, the weight of mice treated with different nano-platform did not show significant changes, and the overall mental state of each mouse remained good (Fig 7d). In order to further evaluate the anti-tumor effect of each nano-platform, H&E and TUNEL staining were used to evaluate the apoptosis and necrosis of cancer cells in tumor tissues (Fig 7e). Compared with PBS and PBS+NIR group, abnormal areas were detected in the treatment groups of ZIF-8/ICG + NIR, MnO_2/ZIF-8/ICG + NIR, and FA-EM@MnO_2/ZIF-8/ICG + NIR. Especially in FA-EM@MnO_2/ZIF-8/ICG + NIR group, more nuclear pyknosis, nuclear lysis and vacuolation was detected in the tumor tissues, which indicated a more significant killing effect on cancer cells. In addition, more green fluorescence detected by TUNEL also confirmed that FA-EM@MnO_2/ZIF-8/ICG + NIR treatment can effectively inhibit the proliferation and induce the apoptosis of cancer cells compared with other treatments. These results indicate that once FA-EM@MnO_2/ZIF-8/ICG nano-platform is exposed to near-infrared radiation, it can effectively inhibit the growth of tumor and reduce unnecessary side effects.

In order to investigate the biocompatibility of FA-EM@MnO_2/ZIF-8/ICG nano-platform to main organs (heart, liver, spleen, lung and kidney), the changes of main organs after 15 d of treatment were detected by H&E staining. It can be seen from Fig. 8 that no obvious toxicity was detected in FA-EM@MnO_2/ZIF-8/ICG group; There was no significant change in H&E staining of tissue sections of different organs.

These results indicated that FA-EM@MnO_2/ZIF-8/ICG nano-platform can be used as a safe and effective nano-platform for tumor treatment.

Conclusion

In summary, we have developed an O_2-generating FA-EM-cloaked ZIF-8 based photosensitizer delivery system (FA-EM@MnO_2/ZIF-8/ICG) for fluorescence-guiding PDT. The constructed FA-EM@MnO_2/ZIF-8/ICG nano-platform has the following merits: 1) It avoids phototoxicity and fluorescence quenching effects of ICG during transportation process; 2) FA-EM@MnO_2/ZIF-8/ICG can avoid eliminated by body immune system and target delivery to tumor tissues;3) by decorated MnO_2 on the surface of ZIF-8, the final FA-EM@MnO_2/ZIF-8/ICG has the ability of self-supplied of O_2 to enhance subsequently PDT. These results proved that FA-EM@MnO_2/ZIF-8/ICG shown excellent biocompatibility, self-sufficiency of O_2 to overcome hypoxia TME further improving the photodynamic activity to therapy tumors, and environment-responsive drugs sustained released. *In vitro* and *in vivo* results illustrated that as-prepared FA-EM@MnO_2/ZIF-8/ICG nano-platform exhibited excellent antitumor effects, which would offer comprehensive effects in tumor therapy and hold great promise for clinical practice.

Abbreviations

ICG: indole green; PDT: photodynamics therapy; TME: tumor microenvironment; ROS: reactive oxygen; NIR: near-infrared; RDPP: $[Ru(dpp)_3]Cl_2$; DPBF: 1, 3-diphenylisobenzofuran; DCFH-DA: 2', 7'-dichlorofluorescein diacetate; TEM: Transmission electron microscope; XRD: X-ray diffraction; MRI: magnetic resonance imaging; CLSM: confocal laser scanning microscopy; DSPE-PEG-FA: 1,2-distearoyl-sn-glycero-3-phosphoethanolamine-N-[folate (polyethylene glycol)-2000]; DAPI: 4’,6-diamidino-2-phenylindole; EM: erythrocyte membrane; FA: folic acid.

Declarations

All authors read and approved the final manuscript.

Ethics approval and consent to participate

All animal experiments are performed according to the protocol approved by the Animal Care Rules and Use Committee of Yangzhou University.

Consent for publication

All authors approved.

Availability of data and material

The datasets generated during and analyzed during the current study are available from the corresponding authors on reasonable request.

Competing interests

The authors declare no conflict of interest.

Funding

This work is supported by Huai'an "Tianyixing" Key Laboratory of Medical Examination (HAP202004).

Authors' contributions

Xinyuan Li and Qing ji made substantial contributions to the conception, paper collecting, and analyzing of the work. Chao Yan and Yan zhihui drafting the work. Yisen Wang final approval of the version to be published. Li Song made substantial contributions to conception of the work; and revising it critically for important intellectual content; and final approval of the version to be published; and agreement to be accountable for all aspects of the work in ensuring that questions related to the accuracy or integrity of any part of the work are appropriately investigated and resolved.

Acknowledgements

This work is supported by Huai'an "Tianyixing" Key Laboratory of Medical Examination (HAP202004).

References

1. Samanta, D.; Park, Y.; Ni, X.; Li, H.; Zahnow, C. A.; Gabrielson, E.; Pan, F.; Semenza, G. L., Chemotherapy induces enrichment of CD47(+)/CD73(+)/PDL1(+) immune evasive triple-negative breast cancer cells. *Proc. Natl. Acad. Sci. USA,* 2018. 115:1239-1248.
2. Fang, L.; Zhao, Z.; Wang, J.; Xiao, P.; Sun, X.; Ding, Y.; Zhang, P.; Wang, D.; Li, Y., Light-controllable charge-reversal nanoparticles with polyinosinic-polycytidylic acid for enhancing immunotherapy of triple negative breast cancer. *Acta Pharm. Sin. B,* 2022. 12: 353-363.
3. Merino, D.; Weber, T. S.; Serrano, A.; Vaillant, F.; Liu, K.; Pal, B.; Di Stefano, L.; Schreuder, J.; Lin, D.; Chen, Y.; Asselin-Labat, M. L.; Schumacher, T. N.; Cameron, D.; Smyth, G. K.; Papenfuss, A. T.; Lindeman, G. J.; Visvader, J. E.; Naik, S. H., Barcoding reveals complex clonal behavior in patient-derived xenografts of metastatic triple negative breast cancer. *Nat. Commun.,* 2019. 10: 766.
4. Jiang, X.; Fan, X.; Zhang, R.; Xu, W.; Wu, H.; Zhao, F.; Xiao, H.; Zhang, C.; Zhao, C.; Wu, G., In situ tumor-triggered subcellular precise delivery of multi-drugs for enhanced chemo-photothermal-starvation combination antitumor therapy. *Theranostics,* 2020. 10: 12158-12173.
5. Wang, H.; Pan, X.; Wang, X.; Wang, W.; Huang, Z.; Gu, K.; Liu, S.; Zhang, F.; Shen, H.; Yuan, Q.; Ma, J.; Yuan, W.; Liu, H., Degradable Carbon-Silica Nanocomposite with Immunoadjuvant Property for Dual-Modality Photothermal/Photodynamic Therapy. *ACS Nano,* 2020. 14: 2847-2859.

6. Zhu, P.; Chen, Y.; Shi, J., Nanoenzyme-Augmented Cancer Sonodynamic Therapy by Catalytic Tumor Oxygenation. *ACS Nano,* 2018. 12: 3780-3795.
7. Zhang, D.; Zhang, J.; Li, Q.; Song, A.; Li, Z.; Luan, Y., Cold to Hot: Rational Design of a Minimalist Multifunctional Photo-immunotherapy Nanoplatform toward Boosting Immunotherapy Capability. *ACS. Appl. Mater. Interfaces,* 2019. 11: 32633-32646.
8. Zhang, H.; Tian, X. T.; Shang, Y.; Li, Y. H.; Yin, X. B., Theranostic Mn-Porphyrin Metal-Organic Frameworks for Magnetic Resonance Imaging-Guided Nitric Oxide and Photothermal Synergistic Therapy. *ACS. Appl. Mater. Interfaces,* 2018. 10: 28390-28398.
9. Hou, M.; Liu, W.; Zhang, L.; Zhang, L.; Xu, Z.; Cao, Y.; Kang, Y.; Xue, P., Responsive agarose hydrogel incorporated with natural humic acid and MnO2 nanoparticles for effective relief of tumor hypoxia and enhanced photo-induced tumor therapy. *Biomater. Sci.,* 2020. 8: 353-369.
10. Gong, Z.; Wang, C.; Wang, C.; Tang, C.; Cheng, F.; Du, H.; Fan, M.; Brolo, A. G., A silver nanoparticle embedded hydrogel as a substrate for surface contamination analysis by surface-enhanced Raman scattering. *Analyst,* 2014. 139: 5283-5289.
11. Pan, H.; Zhang, C.; Wang, T.; Chen, J.; Sun, S. K., In Situ Fabrication of Intelligent Photothermal Indocyanine Green-Alginate Hydrogel for Localized Tumor Ablation. *ACS. Appl. Mater. Interfaces,* 2019. 11: 2782-2789.
12. Hu, D.; Zhang, J.; Gao, G.; Sheng, Z.; Cui, H.; Cai, L., Indocyanine Green-Loaded Polydopamine-Reduced Graphene Oxide Nanocomposites with Amplifying Photoacoustic and Photothermal Effects for Cancer Theranostics. *Theranostics,* 2016. 6: 1043-1052.
13. Tan, X.; Wang, J.; Pang, X.; Liu, L.; Sun, Q.; You, Q.; Tan, F.; Li, N., Indocyanine Green-Loaded Silver Nanoparticle@Polyaniline Core/Shell Theranostic Nanocomposites for Photoacoustic/Near-Infrared Fluorescence Imaging-Guided and Single-Light-Triggered Photothermal and Photodynamic Therapy. *ACS. Appl. Mater. Interfaces,* 2016. 8: 34991-35003.
14. Guo, Y.; Jiang, K.; Shen, Z.; Zheng, G.; Fan, L.; Zhao, R.; Shao, J., A Small Molecule Nanodrug by Self-Assembly of Dual Anticancer Drugs and Photosensitizer for Synergistic near-Infrared Cancer Theranostics. *ACS. Appl. Mater. Interfaces,* 2017. 9: 43508-43519.
15. Cai, X.; Xie, Z.; Ding, B.; Shao, S.; Liang, S.; Pang, M.; Lin, J., Monodispersed Copper(I)-Based Nano Metal-Organic Framework as a Biodegradable Drug Carrier with Enhanced Photodynamic Therapy Efficacy. *Adv. Sci.,* 2019. 6: 1900848.
16. Wan, X.; Zhong, H.; Pan, W.; Li, Y.; Chen, Y.; Li, N.; Tang, B., Programmed Release of Dihydroartemisinin for Synergistic Cancer Therapy Using a CaCO3 Mineralized Metal-Organic Framework. *Angew. Chem. Int. Ed.,* 2019. 58: 14134-14139.
17. Li, Y.; Zhou, J.; Wang, L.; Xie, Z., Endogenous Hydrogen Sulfide-Triggered MOF-Based Nanoenzyme for Synergic Cancer Therapy. *ACS. Appl. Mater. Interfaces,* 2020. 12: 30213-30220.
18. Tian, X. T.; Cao, P. P.; Zhang, H.; Li, Y. H.; Yin, X. B., GSH-activated MRI-guided enhanced photodynamic- and chemo-combination therapy with a MnO2-coated porphyrin metal organic framework. *Chem. Commun.,* 2019. 55: 6241-6244.

19. Wan, S. S.; Cheng, Q.; Zeng, X.; Zhang, X. Z., A Mn(III)-Sealed Metal-Organic Framework Nanosystem for Redox-Unlocked Tumor Theranostics. *ACS Nano,* 2019. 13: 6561-6571.
20. Abdelhamid, H. N., Zeolitic Imidazolate Frameworks (ZIF-8) for Biomedical Applications: A Review. *Curr. Med. Chem.,* 2021, 28: 7023-7075.
21. Wang, Q.; Sun, Y.; Li, S.; Zhang, P.; Yao, Q., Synthesis and modification of ZIF-8 and its application in drug delivery and tumor therapy. *Rsc. Adv.,* 2020. 10: 37600-37620.
22. Zhao, L.; Niu, L.; Liang, H.; Tan, H.; Liu, C.; Zhu, F., pH and Glucose Dual-Responsive Injectable Hydrogels with Insulin and Fibroblasts as Bioactive Dressings for Diabetic Wound Healing. *ACS. Appl. Mater. Interfaces,* 2017. 9: 37563-37574.
23. Xu, W.; Lou, Y.; Chen, W.; Kang, Y., Folic acid decorated metal-organic frameworks loaded with doxorubicin for tumor-targeted chemotherapy of osteosarcoma. *Biomed. Tech.,* 2020. *65*: 229-236.
24. Sun, Q.; Bi, H.; Wang, Z.; Li, C.; Wang, C.; Xu, J.; Yang, D.; He, F.; Gai, S.; Yang, P., O_2-Generating Metal-Organic Framework-Based Hydrophobic Photosensitizer Delivery System for Enhanced Photodynamic Therapy. *ACS. Appl. Mater. Interfaces,* 2019. 11: 36347-36358.
25. Min, H.; Wang, J.; Qi, Y.; Zhang, Y.; Han, X.; Xu, Y.; Xu, J.; Li, Y.; Chen, L.; Cheng, K.; Liu, G.; Yang, N.; Li, Y.; Nie, G., Biomimetic Metal-Organic Framework Nanoparticles for Cooperative Combination of Antiangiogenesis and Photodynamic Therapy for Enhanced Efficacy. *Adv. Mater.,* 2019. 31: 1808200.
26. Fang, Z.; Yang, E.; Du, Y.; Gao, D.; Wu, G.; Zhang, Y.; Shen, Y., Biomimetic smart nanoplatform for dual imaging-guided synergistic cancer therapy. *J. Mater. Chem. B,* 2022. 10: 966-976.
27. Zhang, W.; Yu, Z. L.; Wu, M.; Ren, J. G.; Xia, H. F.; Sa, G. L.; Zhu, J. Y.; Pang, D. W.; Zhao, Y. F.; Chen, G., Magnetic and Folate Functionalization Enables Rapid Isolation and Enhanced Tumor-Targeting of Cell-Derived Microvesicles. *ACS Nano,* 2017. 11: 277-290.
28. Fan, Z.; Li, P. Y.; Deng, J.; Bady, S. C.; Cheng, H., Cell membrane coating for reducing nanoparticle-induced inflammatory responses to scaffold constructs. *Nano Res.,* 2018. 11: 5573-5583.
29. Zeng, F.; Qin, H.; Liu, L.; Chang, H.; Chen, Q.; Wu, L.; Zhang, L.; Wu, Z.; Xing, D., Photoacoustic-immune therapy with a multi-purpose black phosphorus-based nanoparticle. *Nano Res.,* 2020. 13: 3403-3415.
30. Zhang, Z.; Ni, D.; Wang, F.; Yin, X.; Goel, S.; German, L. N.; Wang, Y.; Li, J.; Cai, W.; Wang, X., *In vitro* study of enhanced photodynamic cancer cell killing effect by nanometer-thick gold nanosheets. *Nano Res.,* 2020. 13: 3217-3223.
31. Shen, Y.; Posavec, L.; Bolisetty, S.; Hilty, F. M.; Nystrom, G.; Kohlbrecher, J.; Hilbe, M.; Rossi, A.; Baumgartner, J.; Zimmermann, M. B.; Mezzenga, R., Amyloid fibril systems reduce, stabilize and deliver bioavailable nanosized iron. *Nat. Nanotechnol,* 2017. 12: 642-647.
32. Ren, W.; Yan, Y.; Zeng, L.; Shi, Z.; Gong, A.; Schaaf, P.; Wang, D.; Zhao, J.; Zou, B.; Yu, H.; Chen, G.; Brown, E. M.; Wu, A., A Near Infrared Light Triggered Hydrogenated Black TiO2 for Cancer Photothermal Therapy. *Adv. Healthc. Mater.,* 2015. 4: 1526-36.
33. Sahoo, B.; Devi, K. S.; Dutta, S.; Maiti, T. K.; Pramanik, P.; Dhara, D., Biocompatible mesoporous silica-coated superparamagnetic manganese ferrite nanoparticles for targeted drug delivery and MR

imaging applications. *J. Colloid. Interface Sci.,* 2014. 431: 31-41.

34. Ye, S.; Rao, J.; Qiu, S.; Zhao, J.; He, H.; Yan, Z.; Yang, T.; Deng, Y.; Ke, H.; Yang, H.; Zhao, Y.; Guo, Z.; Chen, H., Rational Design of Conjugated Photosensitizers with Controllable Photoconversion for Dually Cooperative Phototherapy. *Adv. Mater.,* 2019. 31: 1806346.
35. Xiang, H.; Lin, H.; Yu, L.; Chen, Y., Hypoxia-Irrelevant Photonic Thermodynamic Cancer Nanomedicine. *ACS Nano.,* 2019. 13: 2223-2235.
36. Chen, Y.; Xiang, H.; Zhuang, S.; Shen, Y.; Chen, Y.; Zhang, J., Oxygen-Independent Photocleavage of Radical Nanogenerator for Near-IR-Gated and H_2O-Mediated Free-Radical Nanotherapy. *Adv. Mater.,* 2021. 33: 2100129.
37. Bai, J.; Jia, X.; Zhen, W.; Cheng, W.; Jiang, X., A Facile Ion-Doping Strategy To Regulate Tumor Microenvironments for Enhanced Multimodal Tumor Theranostics. *J. Am. Chem. Soc.,* 2018. 140: 106-109.
38. Yu, Z.; Pan, W.; Li, N.; Tang, B., A nuclear targeted dual-photosensitizer for drug-resistant cancer therapy with NIR activated multiple ROS. *Chem. Sci.,* 2016. 7: 4237-4244.
39. Gao, S.; Lin, H.; Zhang, H.; Yao, H.; Chen, Y.; Shi, J., Nanocatalytic Tumor Therapy by Biomimetic Dual Inorganic Nanozyme-Catalyzed Cascade Reaction. *Adv. Sci.,* 2019. 6: 1801733.
40. Fang, Z.; Li, X.; Xu, Z.; Du, F.; Wang, W.; Shi, R.; Gao, D., Hyaluronic acid-modified mesoporous silica-coated superparamagnetic Fe_3O_4 nanoparticles for targeted drug delivery. *Int. J. Nanomedicine,* 2019. 14: 5785-5797.
41. Zou, Q.; Huang, J.; Zhang, X., One-Step Synthesis of Iodinated Polypyrrole Nanoparticles for CT Imaging Guided Photothermal Therapy of Tumors. *Small,* 2018. 14: 1803101.
42. Liu, B.; Hu, F.; Zhang, J.; Wang, C.; Li, L., A Biomimetic Coordination Nanoplatform for Controlled Encapsulation and Delivery of Drug-Gene Combinations. *Angew. Chem. Int. Ed.,* 2019. 58: 8804-8808.
43. Huang, H.; Zhang, C.; Wang, X.; Shao, J.; Chen, C.; Li, H.; Ju, C.; He, J.; Gu, H.; Xia, D., Overcoming Hypoxia-Restrained Radiotherapy Using an Erythrocyte-Inspired and Glucose-Activatable Platform. *Nano Lett.,* 2020. 20: 4211-4219.
44. Deng, J.; Wang, K.; Wang, M.; Yu, P.; Mao, L., Mitochondria Targeted Nanoscale Zeolitic Imidazole Framework-90 for ATP Imaging in Live Cells. *J. Am. Chem. Soc.,* 2017. 139: 5877-5882.
45. Ye, S.; Wang, F.; Fan, Z.; Zhu, Q.; Tian, H.; Zhang, Y.; Jiang, B.; Hou, Z.; Li, Y.; Su, G., Light/pH-Triggered Biomimetic Red Blood Cell Membranes Camouflaged Small Molecular Drug Assemblies for Imaging-Guided Combinational Chemo-Photothermal Therapy. *ACS Appl. Mater. Interfaces,* 2019. 11: 15262-15275.
46. Yan, M.; Liu, Y.; Zhu, X.; Wang, X.; Liu, L.; Sun, H.; Wang, C.; Kong, D.; Ma, G., Nanoscale Reduced Graphene Oxide-Mediated Photothermal Therapy Together with IDO Inhibition and PD-L1 Blockade Synergistically Promote Antitumor Immunity. *ACS Appl. Mater. Interfaces,* 2019. 11: 1876-1885.
47. Liu, W.; Yan, Q.; Xia, C.; Wang, X.; Kumar, A.; Wang, Y.; Liu, Y.; Pan, Y.; Liu, J., Recent advances in cell membrane coated metal-organic frameworks (MOFs) for tumor therapy. *J. Mater. Chem. B,* 2021. 9:

4459-4474.

48. Zhang, L.; Wang, Z.; Zhang, Y.; Cao, F.; Dong, K.; Ren, J.; Qu, X., Erythrocyte Membrane Cloaked Metal-Organic Framework Nanoparticle as Biomimetic Nanoreactor for Starvation-Activated Colon Cancer Therapy. *ACS Nano.,* 2018. 12: 10201-10211.
49. Ren, X.; Zheng, R.; Fang, X.; Wang, X.; Zhang, X.; Yang, W.; Sha, X., Red blood cell membrane camouflaged magnetic nanoclusters for imaging-guided photothermal therapy. *Biomaterials,* 2016. 92: 13-24.
50. Kang, H.; Hu, S.; Cho, M. H.; Hong, S. H.; Choi, Y.; Choi, H. S., Theranostic Nanosystems for Targeted Cancer Therapy. *Nano Today,* 2018. 23: 59-72.
51. Karimi, M.; Eslami, M.; Sahandi-Zangabad, P.; Mirab, F.; Farajisafiloo, N.; Shafaei, Z.; Ghosh, D.; Bozorgomid, M.; Dashkhaneh, F.; Hamblin, M. R., pH-Sensitive stimulus-responsive nanocarriers for targeted delivery of therapeutic agents. *Wiley. Interdiscip Rev. Nanomed Nanobiotechnol,* 2016. 8: 696-716.
52. Wang, S.; Zheng, H.; Zhou, L.; Cheng, F.; Liu, Z.; Zhang, H.; Wang, L.; Zhang, Q., Nanoenzyme-Reinforced Injectable Hydrogel for Healing Diabetic Wounds Infected with Multidrug Resistant Bacteria. *Nano Lett.,* 2020. 20: 5149-5158.
53. Zhang, Y.; Hu, K.; Ling, Z.; Di, W., A MnO_2-$[Ru(dpp)_3]Cl_2$ system for colorimetric and fluorimetric dual-readout detection of H_2O_2. *Rsc. Adv.,* 2010. 9: 7803-7810.
54. Wang, X. H.; Yu, Y. X.; Cheng, K.; Yang, W.; Liu, Y. A.; Peng, H. S., Polylysine modified conjugated polymer nanoparticles loaded with the singlet oxygen probe 1,3-diphenylisobenzofuran and the photosensitizer indocyanine green for use in fluorometric sensing and in photodynamic therapy. *Mikrochim Acta,* 2019. 186: 842.
55. Rajneesh; Pathak, J.; Chatterjee, A.; Singh, S. P.; Sinha, R. P., Detection of Reactive Oxygen Species (ROS) in Cyanobacteria Using the Oxidant-sensing Probe 2',7'-Dichlorodihydrofluorescein Diacetate (DCFH-DA). *Bio. Protoc.,* 2017. 7: 2545.

Scheme 1

Scheme 1 is available in Supplementary Files section.

Figures

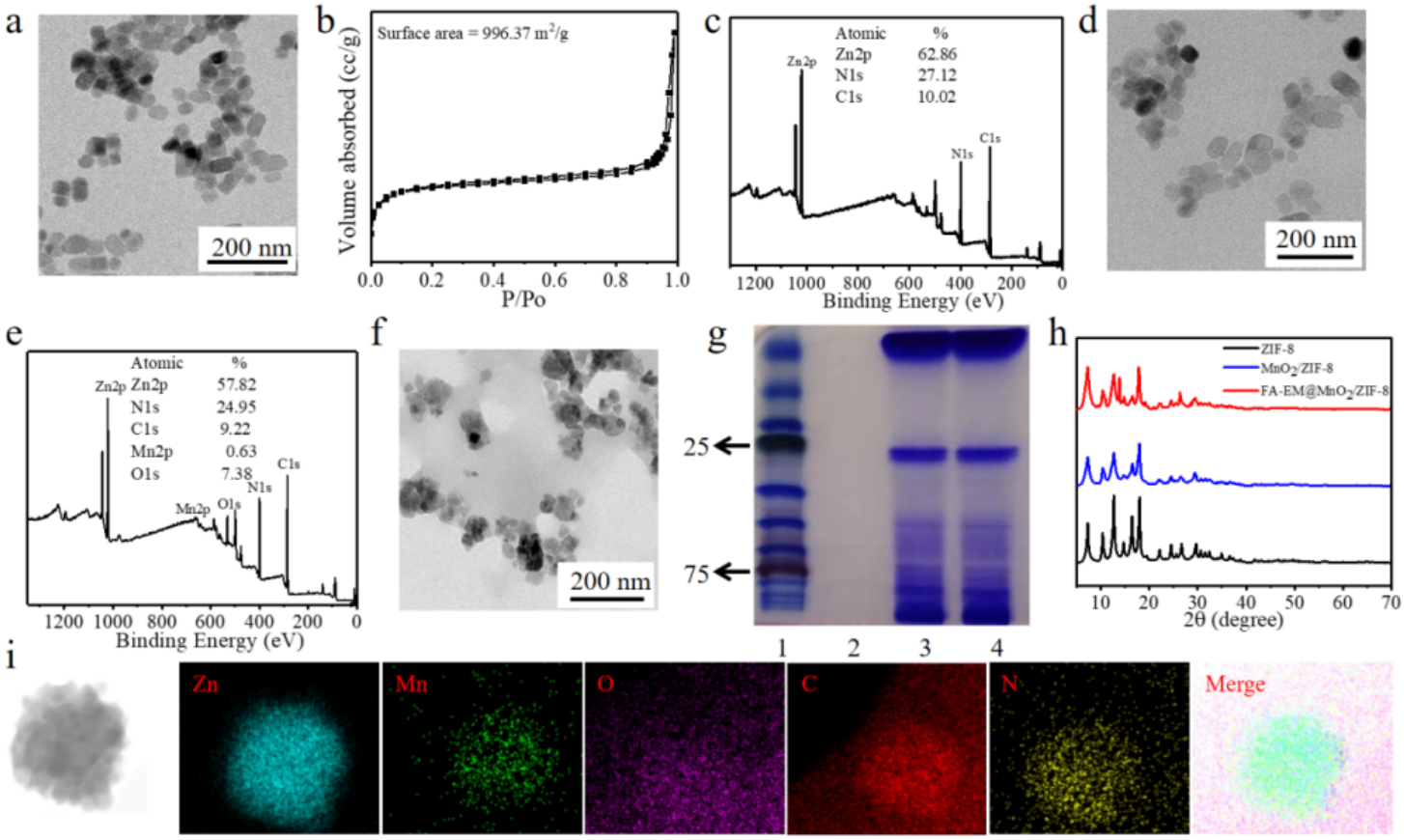

Figure 1

Characterization of FA-EM@MnO_2/ZIF-8 nano-platform. (a) TEM, (b) BET, and (c) XPS of ZIF-8 nano-platform. (d) TEM and (e) XPS of MnO_2/ZIF-8 nano-platform. (f) TEM of FA-EM@MnO_2/ZIF-8 nano-platform. (g) Protein analysis of protein marker (1), MnO_2/ZIF-8 (2), EM (3), and FA-EM@MnO_2/ZIF-8 (4) by using SDS-PAGE. Samples were stained with Coomassie Brilliant. (h) XRD spectra of ZIF-8, MnO_2/ZIF-8, and FA-EM@MnO_2/ZIF-8 nano-platform. (i) High-angle annular dark-field scanning TEM (HAADF-STEM) image and element mapping of FA-EM@MnO_2/ZIF-8 nano-platform.

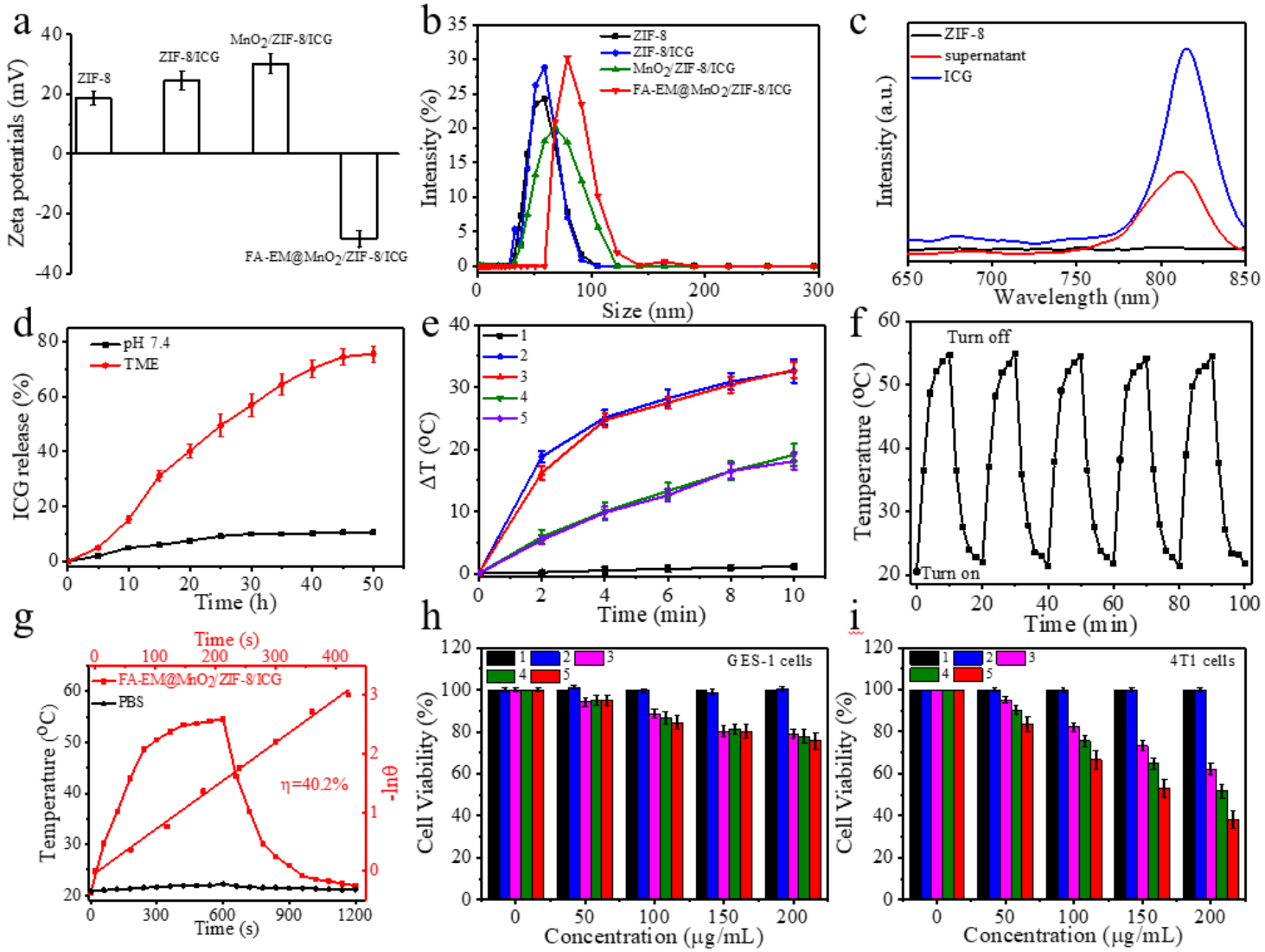

Figure 2

(a) Zeta potential of ZIF-8, ZIF-8/ICG, MnO_2/ZIF-8/ICG and FA-EM@MnO_2/ZIF-8/ICG. (b) Size distribution of ZIF-8, ZIF-8/ICG, MnO_2/ZIF-8/ICG, and FA-EM@MnO_2/ZIF-8/ICG. (c) Fluorescence spectra of ZIF-8, the ICG solution before loading, and the residual ICG in the supernatant after loading. (d) *In vitro* profiles of ICG release from FA-EM@MnO_2/ZIF-8/ICG nano-platform under conditions of pH 7.4 and simulate TME. (e) Temperature changes of PBS (curve 1), 200 μg/mL ZIF-8/ICG (curve 2), 200 μg/mL FA-EM@MnO_2/ZIF-8/ICG (curve 3), and 150 μg/mL FA-EM@MnO_2/ZIF-8/ICG (curve 4) irradiated with 808 nm irradiation (2.0 W/cm^2) for 10 min, and 200 μg/mL FA-EM@MnO_2/ZIF-8/ICG (curve 5) irradiated with 808 nm irradiation (1.5 W/cm^2) for 10 min. (f) Temperature changes of 200 μg/mL FA-EM@MnO_2/ZIF-8/ICG disperse solution irradiation with 808 nm irradiation (2.0 W/cm^2) for five turn on/off cycles. (g) Photothermal response of FA-EM@MnO_2/ZIF-8/ICG solution and H_2O treated with an NIR irradiation (808 nm, 1.5 W/cm^2) for 600s and then the irradiation was turn off. Viability of GES-1 cells (h) and 4T1cells (i) upon treated with PBS (1), PBS + NIR (2), ZIF-8/ICG + NIR (3), MnO_2/ZIF-8/ICG + NIR (4), and FA-EM@MnO_2/ZIF-8/ICG + NIR (5).

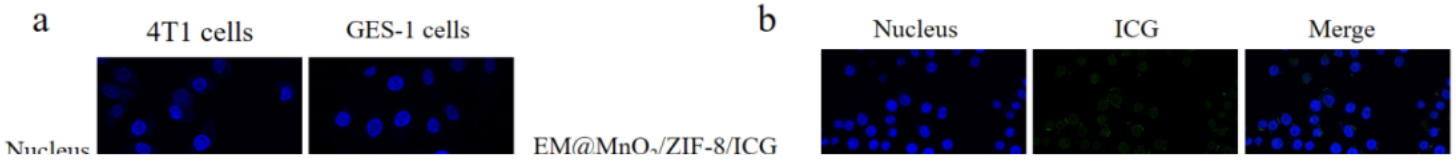

Figure 3

(a) CLSM images of 4T1 and GES-1 cells incubated with FA-EM@MnO_2/ZIF-8/ICG nano-platform for 3 h. (b) CLSM images of macrophage cells incubated with EM@MnO_2/ZIF-8/ICG, FA-EM@MnO_2/ZIF-8/ICG, and MnO_2/ZIF-8/ICG nano-platform for 3 h. Images show cell nuclei stained by DAPI (blue), ICG fluorescence in cells (green) and the merged overlap of the two images. Scale bars: 30 μm.

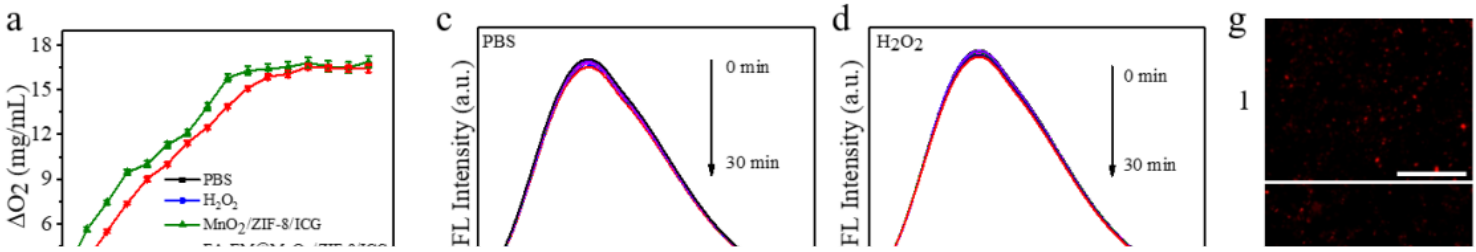

Figure 4

(a) H_2O_2-triggered O_2 generation in different solutions. (b) Photograph of H_2O_2-triggered O_2 generation in different solutions. (A: MnO_2/ZIF-8/ICG in H_2O_2 solution; B: FA-EM@MnO_2/ZIF-8/ICG in H_2O_2 solution; C: MnO_2/ZIF-8/ICG in PBS solution; D: FA-EM@MnO_2/ZIF-8/ICG in PBS solution). (c) Fluorescence spectra of RDPP in PBS (c); H_2O_2 (d); FA-EM@MnO_2/ZIF-8/ICG (e); and FA-EM@MnO_2/ZIF-8/ICG + H_2O_2 (f). (g) CLSM images of RDPP in 4T1 cells without any treatments (1); and treated with H_2O_2 (2); FA-EM@MnO_2/ZIF-8/ICG (3); and FA-EM@MnO_2/ZIF-8/ICG + H_2O_2 (4). Scale bars: 300 μm.

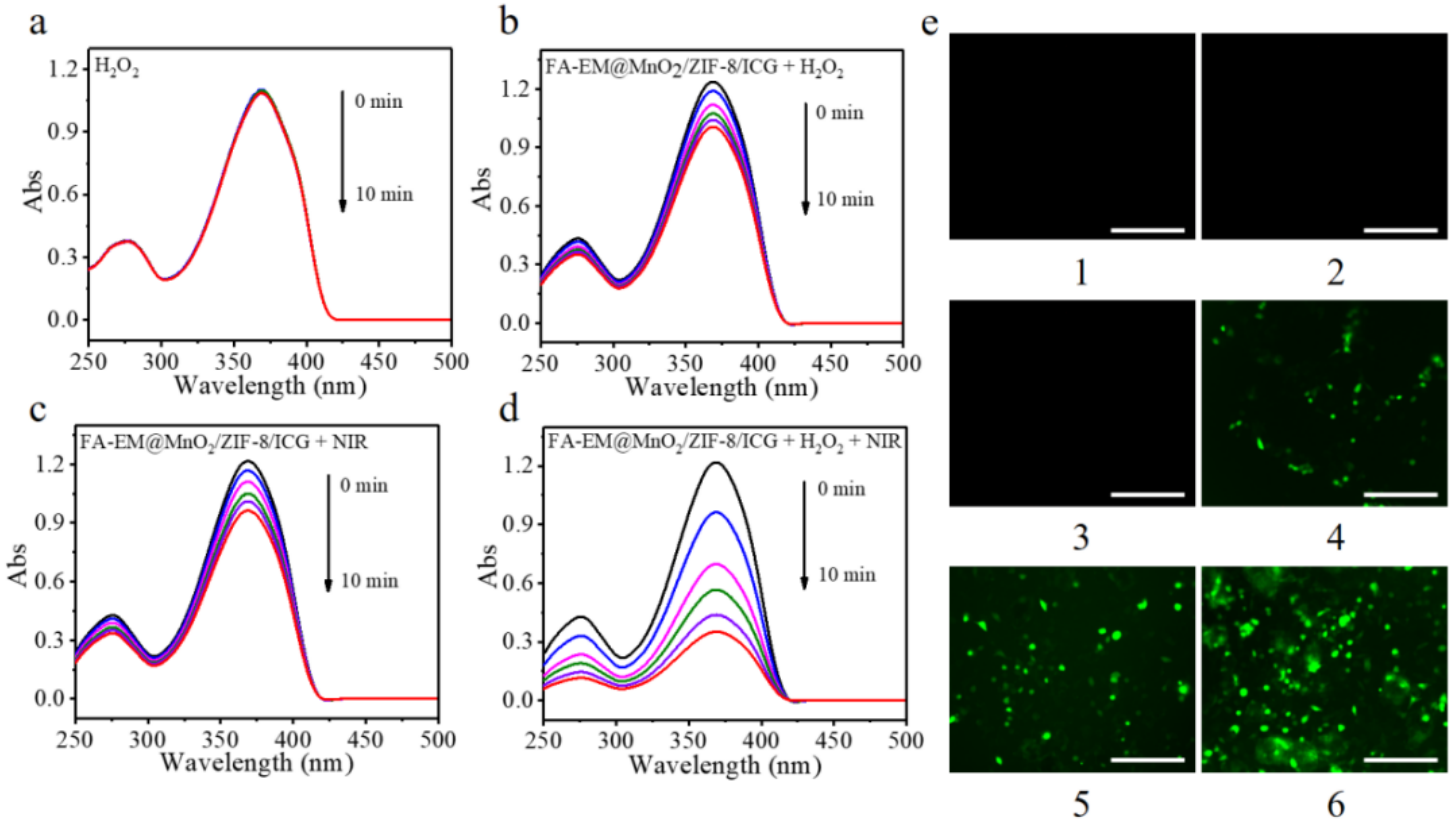

Figure 5

UV-vis absorption of DPBF in H_2O_2 (a), FA-EM@MnO_2/ZIF-8/ICG + H_2O_2 (b), FA-EM@MnO_2/ZIF-8/ICG + NIR (c) and FA-EM@MnO_2/ZIF-8/ICG + H_2O_2 + NIR (d) at different time points. (e) CLSM images of DCF in 4T1 cells without any treatments (1), and treated with NIR irradiation only (2), H_2O_2 (3), FA-EM@MnO_2/ZIF-8/ICG + H_2O_2 (4), FA-EM@MnO_2/ZIF-8/ICG + NIR (5), and FA-EM@MnO_2/ZIF-8/ICG + H_2O_2 + NIR (6). Scale bars: 300 μm.

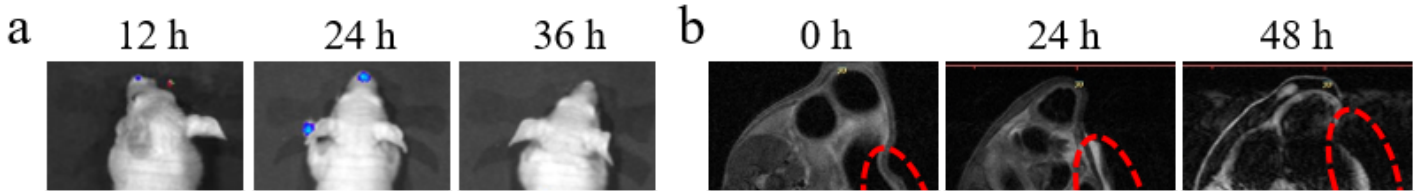

Figure 6

(a) *In vivo* luminescence imaging and (b) MRI of 4T1-bearing mice at designed time after treated with MnO_2/ZIF-8/ICG and FA-EM@MnO_2/ZIF-8/ICG nano-platform.

Figure 7

(a) The tumor volumes in six different groups after treatment. (b) Photographs of the tumors on day 15 post-injection, and (c) Mean tumor weights on day 15 after the last treatment of PBS (1), PBS + NIR (2), ZIF-8/ICG + NIR (3), MnO_2/ZIF-8/ICG + NIR (4), FA-EM@MnO_2/ZIF-8/ICG + NIR (5). (d) Body weight of mice in different groups during treatment. (e) H&E (left) and TUNEL staining (right) of tumor slices collected from 4T1 tumor-bearing mice after treatment of PBS (1), PBS + NIR (2), ZIF-8/ICG + NIR (3), MnO_2/ZIF-8/ICG + NIR (4), FA-EM@MnO_2/ZIF-8/ICG + NIR (5). Scale bars: 100 μm. Significant differences (*: $p < 0.05$; **: $p < 0.01$; ***: $p < 0.001$) among different groups are shown.

Figure 8

Fig 7. H&E staining of various organs collected from 4T1 tumor-bearing mice after different treatments of PBS (1), PBS + NIR (2), ZIF-8/ICG + NIR (3), MnO_2/ZIF-8/ICG + NIR (4), FA-EM@MnO_2/ZIF-8/ICG + NIR (5). Scale bars: 150 μm.

Supplementary Files

This is a list of supplementary files associated with this preprint. Click to download.

- Scheme1.png